Author's Accepted Manuscript

An assessment of the tsunami risk in Muscat and Salalah, Oman, based on estimations of probable maximum loss

John Browning, Neil Thomas
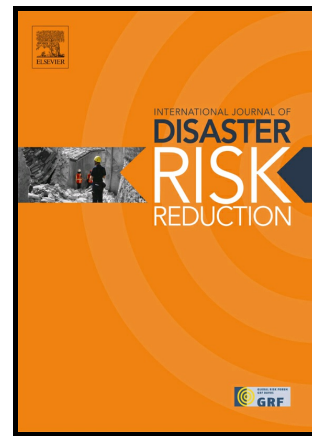
Cite this article as: John Browning and Neil Thomas, An assessment of the tsunami risk in Muscat and Salalah, Oman, based on estimations of probable maximum loss, *International Journal of Disaster Risk Reduction,* http://dx.doi.org/10.1016/j.ijdrr.2016.02.002

An assessment of the tsunami risk in Muscat and Salalah, Oman, based on estimations of probable maximum loss

John Browning[1][2][3] and Neil Thomas[1]

[1] School of Geography, Geology and the Environment, Kingston University, Penrhyn Road, Kingston upon Thames KT1 2EE

[2] Department of Earth Sciences, Royal Holloway, University of London, Egham TW20 0EX

[3] Department of Earth Sciences, University College London, Gower Street, WC1E 6BT

Abstract

We present a method for determining an initial assessment of tsunami risk, with application for two coastal areas of Oman. Using open source GIS and seismic databases we carry out a tsunami risk assessment using a deterministic and probabilistic approach based on worst-case scenarios. A quick and effective method for estimating tsunami run-up without the use of complex modelling software is an important step in disaster risk reduction efforts as many government and emergency response organisations do not possess the expertise to carry out or interpret tsunami inundation numerical models. Estimates of probable maximum loss were calculated using a simple method of building identification and a revised building damage assessment technique. A series of tsunami risk maps were created for the coastal settlements of Muscat and Salalah, with the aim of improving tsunami response. We find Muscat to be at far greater risk of tsunami damage than Salalah; this is due in part to Muscat's proximity to potential tsunamigenic sources and the cities current level of urban infrastructure. Whilst much of the infrastructure in Salalah is currently at low risk from tsunami, development pressures could lead to increased risk within the region. It is hoped that the assessment of risk may go some way to a government led disaster risk reduction strategy being implemented in coastal Oman. The methods detailed provide a cheap and efficient means to quantify tsunami risk in many coastal

Middle Eastern countries, of which several have poor disaster risk reduction strategies.

1. Introduction

Risk assessment is an important component in an end-to-end tsunami early warning system and is therefore a vital contributor to disaster risk reduction. Tsunami modelling can aid the preparation of inundation and evacuation maps required to produce response, recovery and mitigation plans, and educational materials (Crawford, 2006). However, getting government organizations to 'buy in' to disaster risk reduction schemes is not always an easy task. In Oman the organization responsible for Civil Contingencies is the Ministry of Defence and Engineering Services (MODES) with the responsibility of monitoring tsunami falling to the Oman Meteorological Agency (OMA). In recent years, a great emphasis has been, quite rightly, placed on studying tsunami vulnerability with respect to socio-economic, coping and adaptation mechanisms and people-centred warning structures (Post et al., 2007). However, vulnerability is trans-disciplinary and multi-dimensional, covering not only social and economic issues but also political, engineering and ecological aspects. The quantification of vulnerability based on economic damage plays an important role in convincing government organizations of the need for disaster risk reduction, especially for less well saliently perceived hazards such as tsunami.

Here we provide a method for assessing tsunami risk using open access software (Google Earth) combined with simple analytical models, and open access seismic databases used to calculate the probability of tsunamigenesis. Other methods for quick initial assessment of tsunami hazard are available (e.g. Dall'Osso et al., 2010; Wood, 2009), but this is the first study to utilise Google Earth and apply the results to a country within the Middle East, which is a region that has generally received little attention in terms of disaster risk reduction efforts.

1. 1 Tsunami Hazard in the Indian Ocean

Tsunami are responsible for massive loss of life and extensive damage to property in many coastal areas around the world. They are a compelling example of the low probability – high consequence hazard, with on average 2-3 damaging events occurring a year in the global ocean (Dominey-Howes et al., 2006). At many coastal locations the interval between damaging impacts can be hundreds or thousands of years, it is for this reason that tsunami risk is often underestimated. The Boxing Day Indian Ocean tsunami in 2004 which killed more than 225,000 people (Geist et al., 2006) and the Tohoku earthquake and tsunami in 2011 which crippled large parts of Japan (Mori et al., 2011), emphasise the need to study this hazard for various vulnerable coastlines around the world.

Three main types of tsunami hazard assessment have been adopted in the research field. Direct statistical tsunami hazard assessment (DSTHA) uses a large database of tsunami events for a particular region; however such a statistical analysis relies on a comprehensive catalogue of historic events. Many regions such as the Arabian peninsula do not have such a detailed record of historical tsunami, however this method has been used elsewhere by Dominey-Howes et al. (2006) and Orfanogiannaki et al. (2007) for the coasts of Eastern Australia and other Pacific Ocean neighbouring countries. When the studied area does not have the required catalogue of historic tsunami, as is the situation for Oman, a probabilistic tsunami hazard assessment (PTHA) can be conducted using a database of seismic events (Lin and Tung, 1982). However there are areas where seismic activity is minimal and therefore the record of events is small, some of these localities may experience great earthquakes with very long recurrence intervals making the historical tsunami dataset non-existent. In such circumstances a deterministic tsunami hazard assessment (DTHA) can be carried out to model the effects of a worst-case scenario (Geist and Parsons, 2006; Okal et al., 2006).

Tsunami generation in the Arabian Sea has been modelled before but not specifically for the purpose of a tsunami hazard risk assessment and particularly for the coasts of Oman (Heidarzadeh et al., 2007; Heidarzadeh and Kijko, 2011; Heidarzadeh and Satake, 2014). Heidarzadeh et al. (2007) modelled the effects of a range of tsunami events off the southern coast of Iran using deformation algorithms first devised by Mansinha and Smylie (1971). The results showed the average magnitude earthquake for tsunami generation in this region was between Mw 8 to Mw 8.4 (Heidarzadeh et

al, 2014a); such an event could produce a tsunami that would reach the coast of Iran within 15 minutes with wave amplitudes of up to 4 m at locations perpendicular to the fault. There are several tsunami-modelling systems commonly available, ANUGA (Baldock et al., 2007), TSUNAMI-N2 (Goto et al., 1997) and MOST (Titov and Synakolis, 1997). These models generally rely on the quality of a bathymetric dataset for which the Arabian coast is generally poor, and have so far predominantly only focussed on at-risk areas in Australia (Dall'Osso et al., 2014). More recent models have utilised the GEBCO bathymetric dataset to provide probabilistic constraints on the potential amplitude of tsunami in the northwestern Indian Ocean (e.g. Heidarzadeh et al., 2008; Heidarzadeh and Kijko 2011; Heidarzadeh and Satake, 2014).

Coastal Muscat is vulnerable to storm surge and tropical Cyclone flooding, to a degree comparable with distal tsunami such as the 2004 event (Fritz et al., 2010; Belqacem, 2010). Okal et al. (2006) conducted a field survey of the coastal areas of Oman following the Boxing Day 2004 tsunami; their findings showed that Salalah was affected by tsunami wave heights of up to 3.25 m. The damage from this event was minimal and was largely contained to marine and port disruption. A specific example is cited whereby two large container vessels broke free from their moorings at Salalah port.

Oman has experienced historic tsunami, the best documented of which occurred on the 28th November, 1945 when more than 4,000 people were killed in several Arabian Sea neighbouring countries (Pendse, 1946; Sharma et al., 2010). Although no deaths were reported as a direct result of tsunami inundation, several reports from elders indicated a large wave did impact the Oman coast (Jordan, 2008), a claim that is further backed up by tsunami deposits interpreted by Donato et al. (2009) in Sur Lagoon. The 1945 tsunami originated from a thrust fault earthquake that ruptured a along a 100 km length of the Makran Subduction Zone (Byrne and Sykes, 1992). It is this area that is believed to constitute the greatest near field and regional tsunami risk (Heidarzedeh et al., 2007; Mokhtari et al., 2008) (Fig. 1A). The predominant feature that poses a tsunami risk in the far field is the Sunda-Sumatra Megathrust fault (Okal et al., 2008).

1.2 Study areas

1.2.1 Muscat

Muscat is the capital of Oman located on the North Eastern Coast. The area studied is known as 'old Muscat' or more formally the wilyat of Mutrah, bounded by the Port Sultan Qaboos port to the North West and Riyam park to the South East, as shown in Figure 1C. This area is of interest because it is known as one of the main tourist hubs for the country due in part to the many historical landmarks that line the Mutrah corniche, a man made, approximately 3m high sea wall which faces the Port Sultan Qaboos port. The port is the second most important (by export weight) in the Middle East, predominantly due to its location at the mouth of the Strait of Hormuz. The study area is relatively low-lying at the port and surrounding the Corniche, however the town is surrounded on all sides by steep mountainous terrain.

1.2.2 Salalah

Salalah is the capital of the Dhofar region in the South of Oman, with the Port of Salalah an important feature of the economy within this region. In comparison to Muscat, Salalah is relatively low lying and free from mountainous areas. A beach stretches 50km from the Port of Salalah in the West to Taqah in the East, Fig. 1D. Here we focus on the beach area south of Sultan Qaboos Road (Lat 16.59N Lon 54.04E to Lat 17N Lon 54.08E). Salalah has become a major tourist destination attracting over 190,000 visitors per year (Omanet, 2010). The Dhofar region seeks to further boost tourist trade by an increase of 7 percent per annum; this may be accommodated by large franchise beach developments.

1.3 Geological Setting

The geology of the area immediately surrounding Oman is dictated by a complex tectonic regime (Figure 2). The Arabian plate on which Oman is located, moves north-west into the Eurasian plate at a rate of approximately 10 mm y^{-1} (Carayannis, 2006), this continental collision creating the Zagros mountain ranges in western Iran. To the North East of Oman the dominant geological feature is the Makran Subduction

Zone (MSZ), an area that extends from the Gulf of Oman to the Baluchistan Volcanic Arc (Rajedran et al., 2008) approximately 1000 km in length (Heidarzedeh et al., 2008), created by oceanic crust subducting under the Eurasian plate. Convergence between the two plates was estimated by Bryne et al. (1992) to occur at a rate of 40mm yr^{-1}, however this assumed a completely rigid plate motion and has now been more accurately mapped using a network of 27 global positioning stations (Vernant et al., 2004). The result of this mapping shows that in fact subduction occurs at a rate of 19.5 mm yr^{-1}, which in comparison to similar subduction plate boundaries, is particularly slow moving. The Tonga subduction zone is estimated to move at rate of 160 mm yr^{-1} (Bevis et al., 1995), the Japan subduction zone at 80 mm yr^{-1} (Kawasaki et al., 2001) and the Sumatra subduction zone at 65 mm yr^{-1} (Gahaluat and Catherine, 2006).

1.3.1 History of Tsunamis in the Arabian Sea

The record of tsunami in this region is generally poor especially when compared to regions such as Italy, Greece and Japan where a large database of historical and palaeotsunami events exists. There has been no palaeotsunami research or findings in the area adjacent to the Arabian Sea. Three broad assumptions can be made from this observation: 1) large tsunami have not occurred in this region in palaeo time, 2) evidence that does exist has been eroded or developed upon, or 3) a concise effort has not been made to find such deposits. The first of these assumptions seems highly unlikely due to the historical record of tsunami in the region. Whilst this record is still poor, evidence exists to suggest large tsunami have impacted the Omani coast in historical time. As mentioned earlier Donato et al. (2009) attribute deposits found in Sur Lagoon, 200km south of Muscat, to the 1945 tsunami. Deposits are found more than 3 m amsl, which coincides with eyewitness accounts from elders (Donato et al., 2009) and newspaper reports from the time (Pendse, 1946). The 1945 event remains the single most destructive tsunami event originating from the Arabian Sea.

1.3.2 Seismicity on the Makran Subdution Zone (MSZ)

The level of seismicity in the MSZ is considerably lower than what would normally be expected for an oceanic subduction zone. The reasons for such low level seismicity

are hypothesized to be as a result of the relatively low rates of subduction and also the presence of thick sediments and possible high pore pressure within an accretionary wedge (Byrne and Sykes, 1992). The MSZ exhibits a large degree of variance between its eastern and western segments. The Eastern part has experienced 8 large thrust events in historical times whereas the western segment appears relatively aseismic having only experienced two great thrust earthquakes inferred from marine terraces younger than 6,000 years old (Byrne and Sykes, 1992). The reasons for such a behavioural contrast are discussed by Byrne and Sykes (1992); it appears that right lateral strike slip activity is an indication of a separation between the two segments.

Three explanations are offered to account for the low level of seismic activity in the western segment of the MSZ:

1: The western part of the MSZ is locked pending a great earthquake

2: Subduction is taking place almost aseismically

3: Subduction has virtually ceased in the western Makran section

(Musson, 2009)

It is the first of these explanations that is of particular concern since a great thrust earthquake in this section certainly has the potential to be tsunamigenic, but perhaps more worryingly is the possibility of the entire MSZ rupturing in a single Magnitude >8 event.

1.3.3 Morphology of the Makran coast

The Makran subduction zone has one of the world's largest accretionary wedges (Heidarzadeh et al., 2008), characterized by a high sediment thickness of 7km (Koppa et al., 2000 in Heidarzadeh et al., 2008). It is the unconsolidated and semi-consolidated sediments, which make up around 70 km of the seaward forearc (Byrne and Sykes, 1992), which have the potential to fail and produce large submarine tsunamigenic landslides. This massive complex of accretionary material exists due to the break-up of the Arabian and African plates with an increased subduction rate, coinciding with the Himalayan continent-continent collision zone being uplifted and subsequently eroded resulting in an increased input of sediment into the Arabian Sea and Indian Ocean (Mokhtari et al., 2007).

Rajendran et al. (2008) attribute the tsunami of 1945 to a large submarine landslide caused by the Mw 8.1 earthquake. The basis of such an assumption concerns the vast difference in tsunami arrival times at various locations; modelling of the tsunami show that the wave arrived some 17 to 28 minutes later than what should have been expected. Furthermore there was a significant discrepancy (>3 h) between the original earthquake and the arrival of the second tsunami wave.

Tsunami generated by submarine landslides often have very large wave heights close to the source area, but their propagation potential is far less than tsunami generated by earthquakes. The potential for submarine tsunamigenic landslides occurring along the MSZ is difficult to quantify, however it certainly poses an additional hazard. The risk is made even more apparent when it is considered that a smaller magnitude earthquake may be enough to trigger a potentially tsunamigenic submarine slide (Heidarzadeh and Satake, 2014b).

2.1 Simple deterministic tsunami hazard assessment *(DTHA)*

Three separate tsunami scenarios are presented; two originating from the Makran Subduction Zone and one from the Sunda-Sumatra Megathrust, as indicated in Figure 3. For the purpose of modelling, it is assumed that the two Makran source tsunami will not propagate to Salalah efficiently. Furthermore the Sunda-Sumatra source is unlikely to propagate to Muscat. Such an assumption is made based on the 2004 tsunami field survey findings of Okal et al. (2006) where no significant tsunami was found to impact Muscat. Using Google Earth, bathymetry readings were collected for several points in the Indian Ocean (Figure 3) in order to model the speed and amplitude of several hypothetical tsunami. The near shore readings were subdivided to generate a more accurate representation of the continental shelf's effect on velocity and amplitude. The relationship between the velocity (V) of tsunami and ocean depth (d) can be approximated using the shallow water wave equation as:

$$V = \sqrt{(gd)} \qquad\qquad (1)$$

where g is 9.8 m s^{-1}. Amplitude of the tsunami wave at a shoreline (A$_s$) can be inferred from the relationship:

$$V_s/V_d = (A_d/A_s)^{1/2} \qquad (2)$$

where subscripts (s) and (d) correspond to the depth of ocean as simply being shallow (on the continental shelf) or deep (off the continental shelf).

Tsunami wave height at source (A_d) for the purpose of modelling was defined as 0.8m for scenarios 1 and 3, consistent with observations of tsunamis generated by earthquakes with upthrust motions of +/-0.2 m (Gahalaut and Catherine, 2005).

Scenario 2 involves a tsunami generated by a submarine landslide and therefore properties of tsunami propagation and amplitude are calculated differently from scenario 1 and scenario 3. Tsunami characteristics generated by sub-marine landslide are primarily dependant on water depth, landslide volume and acceleration (Murty, 2003). Murty (2003) infers a regression line that can be used to estimate the size of tsunami amplitude (A) based on landslide volume (L):

$$A = 0.3945 \, L \qquad (3)$$

Tsunami amplification factors also need to be considered within the DTHA. Here we use the method of Baldcock et al. (2007) based on a tsunami entering an enclosed V-shape bay with a width-to-length ratio of <0.5; the amplification increase can be as great as a factor of four in worst case scenarios. Based on calculations of the Sultan Qaboos port area in Muscat a maximum W/L ratio of 0.2 is inferred (Figure 4). The bay itself cannot be considered accurately as V-shape but perhaps somewhere between V and U-shape. Therefore based on the shape and W/L ratio an amplification factor of 50% is applied to tsunami impacting this region.

Flat line tsunami inundation, the distance that a tsunami will propagate inland assuming wave height is controlled predominantly by topography, at the two study areas was calculated using topographical data derived from Google Earth. Areas below the tsunami wave height at shore are flooded using this simple modelling technique. Here we consider the maximum wave crest. Whilst the method is a simplification of the dynamics of tsunami run-up and inundation it offers a first order representation of potential tsunami inundation zones based on the height of the tsunami wave versus the local topography.

2.2 Vulnerability Assessment and Indices

The level of tsunami inundation was mapped as a flat line polygon using open source Google Earth software for each scenario event. It is noted that the vertical accuracy of the Digital Elevation Model (DEM) used to create the bathymetric dataset in Google Earth is around 15 m (Ryan et al., 2009). The extent of tsunami inundation represents the physical vulnerability study area. In these zones of maximum run up, an analysis is conducted to determine the specific vulnerability of buildings using a qualitative approach based on the revised Papathoma's Tsunami Vulnerability Assessment (PTVA-3) (Dall'Osso et al., 2009).

It is beyond the scope of this study and the organisational capacity of responsible emergency management organisations to calculate a Relative Value Index (RVI) for each structure. What is conducted is a first order assessment considering the location of structures based on contact with water and general characteristics of building structural vulnerability based on the age, type and height of buildings, examples are shown in Fig. 5.

Whilst there are many ways to characterise building vulnerability and damage (e.g. Wiebe and Cox, 2014; Suppasri et al, 2013) we have chosen to quantify rebuilding cost due to a tsunami impact using a modified method based on Blong's (2003) Building Damage Index (BDI), whereby the cost to rebuild each building is compared to the average price of a House in Oman (Replacement Ratio). We use a figure of OMR 200,000 as the average cost of building a house in Oman (Omanet, 2010). Damage is estimated using the equation:

$$\text{Damage (HE)} = RR \times CDV \qquad (4)$$

where RR is the Replacement Ratio and CDV the Central Damage Value in Omani Rials. Damage is expressed in housing equivalents (HE).

Building use is classified into eight broad categories inferred from Google Earth Imagery. Where building use is not obvious a commercial building classification is provided (RR=1.5). This classification includes any buildings used as shops, souks,

offices and rented apartments. The eight categories included within the building damage assessment include Mosques (RR=6), 1 Storey Residential (RR=0.8), 2 Storey Residential (RR=1.0), 3 Storey Residential (RR=1.2), Hotel (RR=3), Restaurant (RR=1.5) and Café (RR=0.5). Blong's (2003) Index is not specifically designed for use in Middle Eastern countries and therefore a number of buildings are not listed within the classification. We have modified the BDI for use in Oman, buildings such as Mosques have been accounted for based on relative size and common construction materials.

2.3 Probabilistic Tsunami Hazard Assessment (PTHA)

Seismic data from 1973 to 2012 was collected from the USGS NEIC earthquake database using a *rectangular* search query for two fault systems. The Makran Subduction Zone and Sunda-Sumatra Subduction Zone were analysed to investigate the probability of a tsunamigenic event occurring. A filter was applied to ensure results were collected for earthquakes with Magnitudes no less than 3.5 and focal depths no greater than 40 km based on the characteristics of previous tsunamigenic earthquakes.

A non-parametric tool for analysis of survival data called empirical survivor function analysis (Huang, 2008) was assessed to be the best way to calculate a relationship between the magnitude of earthquake events and time. Whilst this analysis does not specifically account for tsunamigenesis, an assumption can be made regarding the competency of a certain magnitude seismic event to generate a tsunami.

Here survivors $(\widehat{S}_i)$ (earthquake events) of a certain magnitude (y) are calculated by considering the number of subjects at risk (n_i) (i.e. still participating in the study before time t_i) and (d_i) the number of subjects (or events) failing at t_i.

$$\widehat{S}_i = \left(\frac{n_i - d_i}{n_i}\right) \widehat{S}_i - 1 \qquad (5)$$

$$\hat{S}_i(y) = \hat{S}_i, t_i \leq y < t_{i+1} \qquad (6)$$

Uncensored data were sorted by Magnitude (y) ≤ 4.0, ≤ 5.0, ≤ 6.0, ≤ 7.0 and then by date of occurrence in a series (t_i). Each category of magnitude earthquake was then

separated and the interval between same magnitude events calculated. Percentages of survival were then calculated for each interval range and plotted as percentage survivors against time in days, from this plot the probability of an event of similar magnitude occurring within an amount of time can be inferred by calculating the inverse of the percentage for the required interval. Therefore using equation (6) S_i is the estimated probability of survival past time (t_i) multiplied by the estimated probability of survival past time t_i given that the event was still alive at time (t_i).

The method presented provides an estimate for the probability of an earthquake occurring following an earthquake of a similar magnitude. Using this method and the last known earthquake, statements can be made relating to the probability of the next potentially tsunamigenic event.

3. Results

All results are presented in the form of deterministic scenarios. In all cases tsunami are modelled from equations 1 and 2, and in all scenarios we describe the tsunamigenic mechanism, and relative tsunami amplitude, speed and timing of events with respect to landfall location.

3.1 Scenario 1 (S1)

Scenario 1 is based on an Mw >8 earthquake occurring off the South coast of Pakistan (Lat 24N Lon 61.34E) caused by a shallow focus (27 km) thrust fault mechanism (Figure 3). A tsunami is produced that impacts the Muscat coastal area within 48 minutes, producing maximum wave heights of 3.4 m (Figure 6). The tsunami is amplified by a factor of 1.5 within Mutrah bay and maximum amplitudes in the corniche reach 5.1 m (Figure 4). The tsunami takes approximately 38 minutes to reach the continental shelf (415 km from source) where it slows dramatically and takes a further 10 minutes to impact the Muscat coast. Tsunami inundation is based upon relative elevation and considers the maximum possible tidal levels (2.8 m) as to simulate the worst case. The tsunami would produce a run up maximum of 7.8 m and inundation maximum of 201 m in the Sultan Qaboos Port area.

Mutrah Corniche would be overtopped in the North and Eastern quadrants where maximum inland inundation extends for approximately 91 m. Al Bahri road would be inundated on both the East and West directions for a length of approximately 1.7 km. Port Sultan Qaboos would be almost completely inundated on the North quadrant of Mutrah bay. We estimate lower run up values for the outer-most walls of Port Sultan Qaboos because the wave will not be amplified to the same extent in these locations. An area of approximately 3.7 km^2 along the Mutrah Corniche is overtopped. Reconstruction cost resulting from tsunami inundation, based on an S1 tsunami, equates to OMR 6,924,000 (Table 1).

3.2 Scenario 2 (S2)

This scenario is based on an Mw 6.5 Earthquake occurring on the western segment of the Makran Subduction Zone (Lat 24.40N Long 58E) at a focal depth of 15 km (Figure 7). The initial earthquake does not trigger a tsunami but 17 minutes later (in our hypothetical simulation) a large submarine landslide with a volume of ~20 million m^3 occurs producing a tsunami at source of 1.2 m. The tsunami propagates towards the Muscat coast developing to a height of 4.3 m within 20 minutes. The initial tsunami enters Mutrah bay 24 minutes after the landslide occurs, amplifying to a height of 6.5 m (Figure 7).

An S2 tsunami provides significantly higher run-up values to that observed for an S1 event and in turn produces a higher degree of physical damage. As there are a number of landmark features in the Mutrah area (Table 2) it can be assumed that a number of tourists will be present in the bay area; the risk posed to tourists is also increased due to the number of hotels located near the Corniche. Port Sultan Qaboos could be disrupted for several weeks following inundation from a tsunami based on either scenario S1 or S2.

3.3 Scenario 3 (S3)

This scenario is based on an Mw >9 earthquake occurring off the SW coast of Padang, Indonesia (Lat 0.59S Lon 97.54E) at a focal depth of 25 km (Figure 3). The resultant

tsunami takes approximately eight hours to reach the South Eastern coast of Oman producing maximum wave heights of 3.5 m at Salalah (Figure 8). The tsunami wave slows as it reaches the Southern Indian continental shelf and again as it passes the Murray Ridge in the Arabian Sea. This has implications for arrival times as the tsunami takes approximately two hours to pass these sections.

Maximum inundation of 0.5 m is observed to the eastern side of the study area where a natural inlet has the potential to amplify wave height by a factor of 1.2 (Figure 8). This is a particular area of concern due to the proximal location of the Al Baleed historical monuments. Results show that certain locations within the historical site are inundated to a depth of 0.5 m. The damage resultant from such flooding is difficult to quantify but the site is an area of tourist interest and as a result the region's economy may suffer. Physical damage is limited predominantly to structures directly facing the beach (Table 3) although several areas adjacent to the main beach are inundated and therefore risk in these areas is calculated to be high.

3.5 Probability of occurrence

Here we assess the probability of tsunamigenic earthquakes in the Oman region, i.e. those Earthquakes of magnitude >7. We find from analysis of survivor functions that there is a ~70% chance of a tsunamigenic earthquake occurring from the Sunda-Sumatra fault within 3 years of a similar magnitude event. Within a shorter timeframe, for example 1 year, there is a ~50% likelihood of a tsunamigenic earthquake occurring from the Sunda-Sumatra fault. Following a large magnitude earthquake, a region is less likely to experience an event of similar magnitude in a short period of time. A magnitude >6 event on the Sunda-Sumatra fault would be highly likely to occur within a few weeks following a similar magnitude event based on the analysis of survivor functions.

The thirty-seven year earthquake record used for the Makran Subduction Zone does not adequately display any trends for use in calculating tsunami probability, this is because no large magnitude events have occurred during this time and as result neither have any tsunami. It is perhaps more appropriate to use Byrne and Sykes

(1992) estimate of a 200-300 year return period for large thrust earthquakes occurring on the eastern Makran Subduction Zone. The western segment of this fault line may produce great thrust earthquakes with much larger return periods, of which it is difficult to speculate a probability.

4. Discussion

Risk zones (Figure 9) are approximated by the accumulation of probable tsunami inundation calculated from our worst-case scenario models and the exposure of buildings to these tsunami inundation zones. Areas lying adjacent to tsunami inundation are generally assigned medium to low risk. Risk has only been calculated for the zones in Figure 9, this is not to suggest that the areas outside of these zones have no associated risk. Certain locations are not necessarily inundated by tsunami but can still be considered at high risk. This is for two reasons, 1) the locality is on higher ground surrounded by low-lying areas where inundation takes place, meaning access will be cut off. 2) The locality is densely populated or has higher value buildings and therefore more vulnerable.

Salalah is predominantly at low risk (Figure 9), however all beach areas are calculated as being at high risk from inundation. Increasing development in beachfront areas may further increase risk over time. The greatest risk is observed on the eastern side of the study area where the Al Baleed natural park and historical monuments are located.

Muscat is considered to be predominantly at high risk due to a combination of the proximity of tsunamigenic sources and the location of infrastructure and people around Mutrah bay. It can be observed that the low and medium risk parts of the city are relatively narrow sections, this is because low lying and high risk areas are quickly replaced by steep mountains where inundation would not be expected to take place therefore quickly reducing risk.

4.1 Limitations

4.1.1 Tsunami Modelling

Tsunami wave height and travel time estimation is limited by the accuracy of Google Earth derived bathymetry datasets and also the number of bathymetric readings used. Google Earth provides bathymetry resolution uncertainty of approximately 15 m. Ideally, a tsunami would be modelled based on a much higher resolution bathymetric dataset and therefore each tsunami inundation zone would represent a different depth value, however the user interface of Google Earth makes such an analysis virtually impossible. The final inundation figure provided is based on a flat line value with maximum run up defined by ground topography, however a preferable method would have modelled in detail the movement and interaction of water with buildings and roads. Several qualitative details are noted which may impact the flow of water in the study areas, such as the roads within Mutrah corniche which run perpendicular to the bay, this road layout may further amplify waves and increase maximum wave run up.

Tsunami propagation is largely dependent on the direction of fault displacement (Heidarzedeh et al., 2008), in the first scenario, Muscat is located in an oblique direction to the fault therefore minimising tsunami propagation potential in this direction. Specific directional propagation is not accounted for in these models, however it is noted that it is most likely that fault displacement in S1 would occur in a E-W direction, therefore maximising effects in a N-S direction.

4.1.2 Vulnerability Assessment

The method of identifying structural types and location can be used as a first order approximation of structural vulnerability, for remote or difficult to access areas which may be relevant for regions in southern Iran for example. Ideally any remotely sensed data would be grounded truthed but this is not an option and leads to large and perhaps unnecessary expense when considering the purpose of the assessment is partly when of economising the process.

There are a number of potential problems which arise from using software like Google Earth to infer building types and locations, for example pictures uploaded to Google Earth are not subject to verification and therefore their location and description can be misleading. Furthermore, in Salalah the database of pictures is much less than that of Muscat. Many of these problems were overcome by identifying the correct location of pictures based on landmark features such as mosques and road

layouts. Here we do not attempt to make an assessment of social vulnerability, in terms of populous but simply exposure to risk.

5. Conclusions

We have introduced a method of tsunami risk quantification using open source databases and software. Such a technique should be useful for Civil Protection and Emergency Management organisations within developing countries as a first order tsunami risk identification tool. The use of imagery within open source GIS software such as Google Earth can be a powerful tool for making inferences about the likely damage and loss experienced during a range of tsunami or other hazard events. As a first order approximation of the likely tsunami travel times and inundation levels simple models can be used to illustrate the state of risk in coastal communities. This is especially salient for areas which lack a detailed bathymetric dataset.

Tsunami pose a risk to Oman's eastern and northern coast from two predominant source regions. It is the Makran Subduction Zone that constitutes the greatest risk to the Northern coastline (Heidarzadeh et al., 2009; Heidarzadeh and Kijko, 2011; Heidarzadeh and Satake, 2014b), here a locally generated tsunami has the potential to impact the capital Muscat within 20 minutes. The devastation caused by such an event would be unprecedented in Oman's history of natural disasters. Whilst this type of tsunami may appear improbable due to the relative lack of seismic activity on the western MSZ, several possibilities have been discussed that should be of concern, among the most salient is the possibility of a large sub marine landslide generating an over 9 m high tsunami. An earthquake event occurring in the eastern MSZ would produce a tsunami that takes over 45 minutes to reach Muscat; this should be enough time to evacuate at risk areas assuming an evacuation plan and warning system is in place.

Salalah is found to be at a low risk from tsunami inundation. the predominant concern in this region is for low lying beach areas where no personal announcement (PA) system is currently in place to warn of an impending tsunami. If such a system was installed, together with the Indian Ocean tsunami warning system, evacuation time would be up to 8 hours, potentially sufficient time to evacuate high risk locations. The physical damage for a worst case scenario tsunami impacting Salalah is minimal as

many of the structures are built away from the beach, however development in this area may significantly increase vulnerability in the future as developments are built in high risk zones. It is believed careful planning should be conducted to ensure the low risk from tsunami in this region does not increase due to development pressures.

Acknowledgements

6. References

Baldock, T.E; Barnes, M.P; Guard, P.A; Hanslow, D; Ranasinghe, R; Gray, D; Nielsen, O. 2007. Modelling tsunami inundation on coastlines with characteristic form. *16th Australasian fluid mechanics conference (AFMC)*

Belqacem, M., 2010, Urban sprawl and City vulnerability: Where does Muscat Stand?. *Indian Ocean Tropical Cyclones and Climate Change.* 233-243

Bevis, M; Taylor, F.W; Chutz, B.E; Recy, J; Isacks, B.L; Helu, S; Singh, R; Kendrick, E; Stowell, J; Taylor, B; Calmant, S., 1995. Geodetic observations of very rapid convergence and back-arc extension at the Tonga arc. *Nature.* **374**, 249-251

Blong, R. 2003. A New Damage Index. *Natural Hazards.* **30**: 1-23

Byrne, D.E and Sykes, L.R. 1992. Great Thrust Earthquakes and Aseismic Slip along the plate boundary of the Makran Subduction Zone. *Journal of Physical Research.* **97**. 449-478

Carayannis, G.P. 2006. The potential of Tsunami generation along the Makran Subduction Zone in Northern Arabian Sea. Case Study: The earthquake and tsunami of November 28, 1945. *Science of Tsunami Hazards*, **24**, 358-384

Crawford, G.L. 2006. Developing tsunami ready communities: translating scientific research into useable emergency management products. *EERI*. p1-8

Dall'Osso, F; Dominey-Howes, D; Moore, C; Summerhayes, S; Withycombe, G 2014. The exposure of Sydney (Australia) to earthquake-generated tsunamis, storms and sea level rise: a probabilistic multi-hazard approach. *Scientific reports*. **4**. 7401

Dall'Osso, F; Gonella, M; Gabbianelli, G; Withycombe, G; Dominey-Howes, D. 2009. A revised (PTVA) model for assessing the vulnerability of buildings to tsunami damage. *Nat Hazards Earth Sys Sci.* **9**. 1557-1565

Dall'Osso,F; Bovio, L; Cavalletti, A; Immordino, F; Gonella, M; Gabbianelli, G. 2010. A novel approach (the CRATER method) for assessing tsunami vulnerability at the regional scale using ASTER imagery. *Italian Journal of Remote Sensing* **42** (2), 55-74

Dominey-Howes, D; Cummins, P; Burbidge, D. 2006. Historical Records of teletsunami in the Indian Ocean and Insights from numerical modeling. *Nat. Hazards*.

Donato, S.V; Reinhardt, E.G; Boyce, J.I; Pilarczyk, J.E; Jupp, B.P. 2009. Particle-size distribution of inferred tsunami deposits in Sur Lagoon, Sultanate of Oman. *Marine Geology.* **257**. 54-64

EM-DAT, 2010. Disaster Profile – Oman. > accessed 20/4/10

Fritz, H.M; Blount, C; Albusaidi, F.B; Al-Harthy, A.H.M. 2010. Cyclone Gonu Storm Surge in the Gulf of Oman. *Indian Ocean Tropical Cyclones and Climate Change.* 255-263

Gahalaut, V.K and Catherine, J.K. 2005. Rupture Characteristics of 28 March 2005 Sumatra Earthquake from GPS measurements and its implications for tsunami generation. *Earth and Planetary Science Letters*. **249**. 39-46.

Geist, E., Titov, V., Synolakis, C., 2006. Tsunami: wave of change. *Scientific American*, 56–63.

Geist, E and Parsons. T 2006. Probabilistic Analysis of tsunami hazards. *Natural Hazards*. **37**. 277-314

Greene, R.W 2002. *Confronting Catastrophe, A GIS Handbook.* ESRI press. Redlands California. Pp135

Gotu, C; Ogawa, Y; Shuto, N; Imamura, F. 1997. Numerical method of tsunami simulation with leap-frog scheme (IUGG/IOC Time Project), IOC Manual, UNESCO, No.35

Heidarzadeh, M, Zaker, N.H, Pirooz, M.D, Mokhtari, M. 2007. Modelling of tsunami propagation in the vicinity of the southern coasts of Iran. *Proceedings of the 28th International Conference on Offshore Mechanics and Arctic Engineering.* San Diego

Heidarzadeh, M; Pirooz, M.D; Zaker, N.H; Yalciner, A.C. 2008. Preliminary estimation of the tsunami hazards associated with the Makran subduction zone at the northwestern Indian Ocean. *Natural Hazards.* **48**. 229.243

Heidarzadeh, M; Pirooz, M.D; Zaker, N.H. 2009. Modelling the near-field effects of the worst case tsunami in the Makran subduction zone. *Ocean Engineering.* 1-9

Heidarzadeh, M. and Kijko, A. 2011 A probabilistic tsunami hazard assessment for the Makran subduction zone at the northwestern Indian Ocean, *Natural hazards* 56 (3), 577-593.

Heidarzadeh, M. and Satake, K. 2014a. New insights into the source of the Makran tsunami of 27 November 1945 from tsunami waveforms and coastal deformation data, *Pure and Applied Geophysics*, 172 (3), 621-640.

Heidarzadeh, M. and Satake, K. 2014b. Possible sources of the tsunami observed in the northwestern Indian Ocean following the 2013 September 24 Mw 7.7 Pakistan inland earthquake, *Geophysical Journal International* 199 (2), 752-766.

Huang, M.L. 2008. A weighted estimation method for survival function. *Applied Mathematical Sciences* Vol 2. **16**. 753-762

Jordan, B.R. 2008. Tsunamis of the Arabian Peninsula a Guide of Historic Events. *Science of Tsunami Hazards.* **27**, 31

Kawasaki, I; Asai, Y; Tamura, Y. 2001. Space-time distribution of interplate moment release including slow earthquakes and the seismo-geodetic coupling in the Sanriku-oki region along the Japan trench. *Techonophysics.* **330**, 267-283

Koppa, C; Fruehn, J; Flueh, E.R; Reichert, C; Kukowski, N; Bialas, J. 2000. Structure of the Makran Subduction Zone from wide-angle and reflection seismic data. *Tectonophysics*. **329**: 171-191

Lin, I. C. and Tung, C. C. (1982), A preliminary investigation of tsunami hazard, B. Seismol. Soc. Am. **72** (6), 2323–2337.

Mansinha, L and Smylie, D.E. 1971. The Displacement field of inclined faults. *Bulletin of seismological society of America.* **6**: 1433-1440

Mokhtari, M. 2007. Seismological Aspect and Ews of Tsunami prone area of Iranian coasts with special emphases on Makran (Sea of Oman).

Mokhtari, M; Fard I.A; Hessami, K. 2008. Structural elements of the Makran region, Oman sea and their potential relevance to tsunamigenisis. *Natural Hazards.* **47**. 185-199

Mori, N; Takahashi, T; Yasuda, T; Yanagisawa, H. 2011. Survey of 2011 Tohoku earthquake tsunami inundation and run-up. *Geophysical research letters.* 38. doi:10.1029/2011GL049210.

Musson, R.M.W. 2009. Subduction in the Western Makran: The historian's contribution. *BGS Report.* 1-18.

Murty, T.S. 2003. Tsunami Wave Height Dependence on Landslide Volume. *Pure and Applied Geophysics*. **160**. 2147-2153

Okal, E.A., Fritz, H.M., Raad, E.P., Synokalis, C.E., Al-Shijbi, Y., and AL-Saifi, M. 2006), Oman field survey after the December 2004 Indian Ocean tsunami, *Earthq. Spectra* **22** (S3), S203–S218.

Okal, E. A. and Synolakis, C. E. 2008, Far-field tsunami hazard from mega-thrust earthquakes in the Indian Ocean, *Geophys. J. Int*. **172** (3), 995–1015.

Omanet. 2010. Ministry of Information, Sultanate of Oman. <www.omanet.om> accessed 14/12/09

Orfanogiannaki, K and Papadopoulos, G.A. 2007. Assessment of Tsunami potential: Application in three tsunamigenic regions of the Pacific Ocean. *Pure and Applied Geophysics.* **164**. 593-603

Pendse, C.G. 1946. The Mekran Earthquake of the 28th November 1945. *Scientific Notes.* Vol. X, No.125

Post, J; Zosseder, K; Strunz, G; Birkmann, J; Gebert, N; Setiadi, N; Anwar, Z; Harjono, H; Nur, M; Siagian, T. 2007. Risk and vulnerability assessment to tsunami and coastal hazards in Indonesia: Conceptual framework and indicator development. *GITEWS project.* No 15

Rajedran, C.P, Ramanamurthy, M.V, Reddy, N.T, Rajendran, K. 2008. Hazard implications of the late arrival of the 1945 Makran tsunami. *Current Science.* **95**.12. 1739-1743

Ryan, B.F, Carbotte, S.M, Coplan, J.O. 2009. Global Multi-Resolution Topography synthesis. **10**. 1525-2027

Sharma, P.K; Ghosh, B; Singh, R.K; Ghosh, A.K; Kushwaha, H.S. 2010. Initial Numerical Assessment of Tsunami Due to 1945 Makran Earthquake. *Bhabha Atomic Research.* 1-7

Suppasri, A., Mas, E., Charvet, I., Gunasekera, R., Imai, K., Fukutani, Y., Abe, Y. and Imamura, F. 2013, Building damage characteristics based on surveyed data and fragility curves of the 2011 Great East Japan tsunami, Nat. Hazards, 66 (2), 319-341.

Titov, V and Synakolis, G 1997. Extreme inundation flow during the Hokkaido-Nansei-Oki tsunami. *Geophysical Research Letters*. **24**, 1315-1318

Vernant, P.H; Nilforoushan, F; Hatzfield, D; Abbasi, M.R; Vigny, C; Masson, F; Nankali, H; Martinod, J; Ashtiani, A; Bayer, R; Tavakoli, F; Chery, J. 2004. Present-Day Crustal deformation and plate kinematics in the Middle East constrained by GPS measurements in Iran and Northern Oman. *Geophys. J. Int.* **157**: 381-398

Wiebe, D. M. and Cox, D. T. 2014 Application of fragility curves to estimate building damage and economic loss at a community scale: a case study of Seaside, Oregon, *Nat. Hazards*, 71 (3), 2043-2061.

Wood, N., 2009, Tsunami Exposure Estimation With Land Cover Data: Oregon And The Cascadia Subduction Zone. *Applied Geography*.

Figures

Figure 1. Potential Indian ocean tsunamigenic sources, red indicates subduction zones, blue spreading ridges, green partly strike slip faults, and orange volcanic centres. B) Coastal Oman where Muscat and Salalah are indicated. C) Greater Muscat area, Mutrah the area of study is located approximately 3.5km west of old Muscat. D) Southern Dhofar region of Salalah.

Figure 2. Tectonic setting of the Arabian Sea and surrounding area, the Makran Subduction zone and associated accretionary complex represents the predominant tsunamigenic source in the region, modified after Mokhtari et al (2008)

Figure 3. Projections showing the shortest straight line distance between tsunamigenic source area and towns studied. Depth and tsunami height models were made approximately every 100 km along these lines. A) Scenario 1 and 2

associated with thrust faulting and submarine landslides on the Makran Subduction Zone and B) Scenario 3, a megathrust event on the Sumatra fault.

Figure 4. Structure of the Sultan Qaboos port area in Muscat. Maximum width to length ratios (given in red) are observed nearest the Corniche wall where tsunami amplification will be greatest.

Figure 5: Google Earth imagery and database used to infer building types and locations in Muscat. Source GoogleEarth, 2014. Example of imagery used from Google Earth to infer building type and location for estimation of physical vulnerability. Source Google Earth, 2014

Figure 6. Estimated tsunami amplitude and arrival times in Muscat, maximum tsunami amplitude is multiplied by 1.5 to compensate for likely funnelling effects. The map below plots the maximum inundation from a worst case scenario 1 tsunami impact.

Figure 7. Estimated tsunami amplitude and arrival times in Muscat, maximum tsunami amplitude is multiplied by 1.5 to compensate for likely funnelling effects. The map below plots the maximum inundation from a worst case scenario 2 tsunami impact, considering a sub-marine landslide generation mechanism.

Figure 8. Maximum inundation in Salalah resulting from a scenario 3 tsunami originating from the Sunda-mega thrust.

Figure 9. Deterministic risk maps of Muscat based on scenario 1 (A) and scenario 2 (B) and Salalah, scenario 3 (C). Red indicates high risk and yellow, low risk, the orange zone indicates the transition between areas at most and least risk within the study area.

Tables

Table 1. Replacement costs resulting from an S1 tsunami

Building Type	No. of Buildings	Replacement Ratio (RR)	Central Damage Index (CDI)	House Equivalents (HE)
Mosque	2	6.0	0.50	6.00

Building Type	No.	RR	CDI	HE
1 Storey Residential	3	0.8	0.75	1.80
2 Storey Residential	4	1.0	0.40	1.60
2 Storey Residential	7	1.0	0.75	5.25
3 Storey Residential	7	1.2	0.40	3.36
Small Hotel	3	2.0	0.40	2.40
Medium Hotel	3	2.5	0.35	2.63
Large Hotel	1	3.0	0.35	1.05
Restaurant	2	1.4	0.70	1.96
Café	5	0.5	0.70	1.75
Commercial Non Specific	13	1.5	0.35	6.83

|	HE	34.62
	Rebuild Cost	OMR 6,924,000

Table 2. Replacement costs resulting from an S2 tsunami

Building Type	No. of Buildings	Replacement Ratio (RR)	Central Damage Index (CDI)	House Equivalents (HE)
Mosque	4	6	0.75	18
1 Storey Residential	7	0.8	1	5.6
1 Storey Residential	4	0.8	0.75	2.4
2 Storey Residential	13	1	0.4	5.2
2 Storey Residential	5	1	0.75	3.75
2 Storey Residential	15	1	1	15
3 Storey Residential	12	1.2	0.75	10.8
Small Hotel	7	2	0.75	10.5
Medium Hotel	6	2.5	0.65	9.75
Large Hotel	3	3	0.5	4.5
Restaurant	12	1.4	0.7	11.76
Café	18	0.5	0.7	6.3
Commercial Non Specific	34	1.5	0.5	25.5

|	HE	129.06
	Rebuild Cost	OMR 25,812,000

Table 3. Replacement costs resulting from an S3 tsunami

Building Type	No. of Buildings	Replacement Ratio (RR)	Central Damage Index (CDI)	House Equivalents (HE)
1 Storey Residential	7	0.8	0.25	1.40
2 Storey Residential	2	0.8	0.2	0.32
Hotel	1	4	0.1	0.40
Restaurant	1	1.4	0.2	0.28
Café	1	0.5	0.2	0.10
Commercial Non Specific	9	1.5	0.25	3.38

HE	5.88
Rebuild Cost	OMR 1,175,000

Iran

Pakistan

Makran
subduction zone

Muscat

Oman

Owen
fracture zone

Salalah

India

Sri
Lanka

Andaman
Nicobar

Sunda-Sumatra

Chagos archipelago

1000 km

N

B

Oman

C

D

200 km

N

C

Sultan Qaboos port

Muscat

2 km

N

D

Salalah

Taqah

Port of Salalah

2 km

N

Corniche

N

370 m

240 m

700 m

1100 m

Ratio = 0.5

Ratio = 0.2

100 m   580 m

Ratio = 5.8
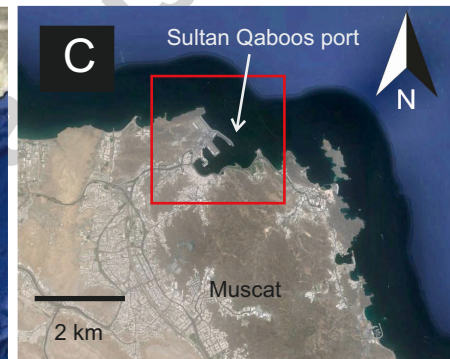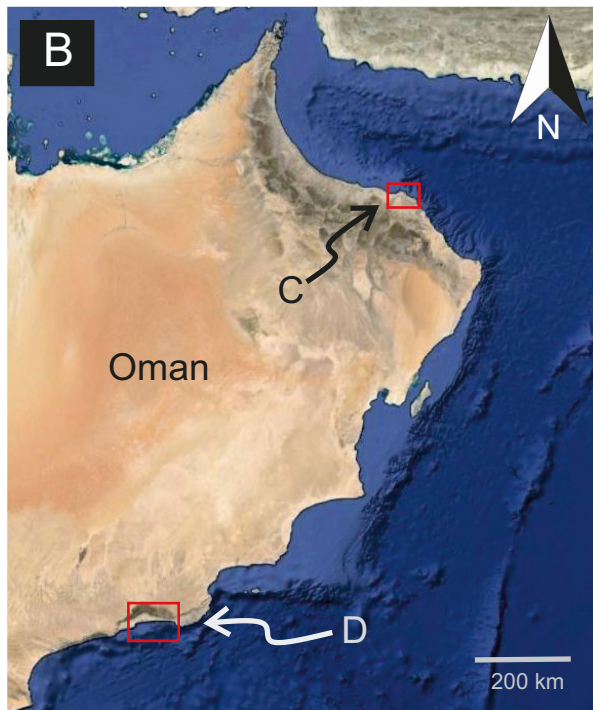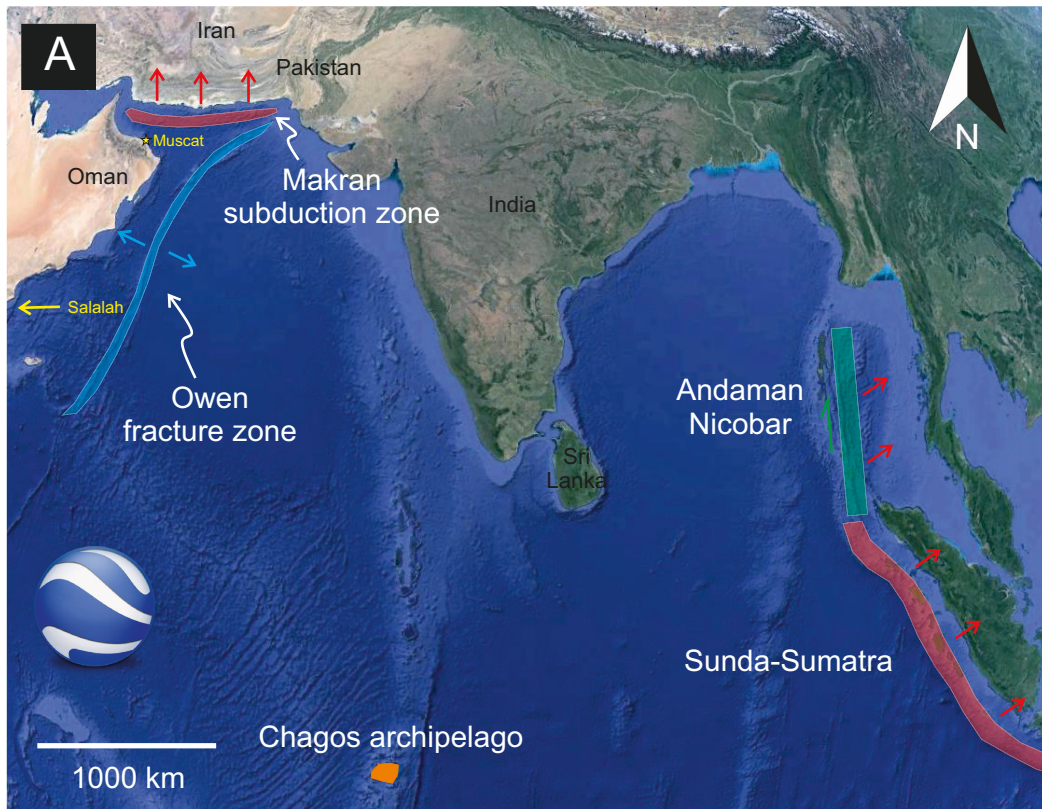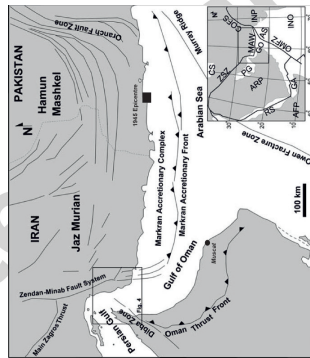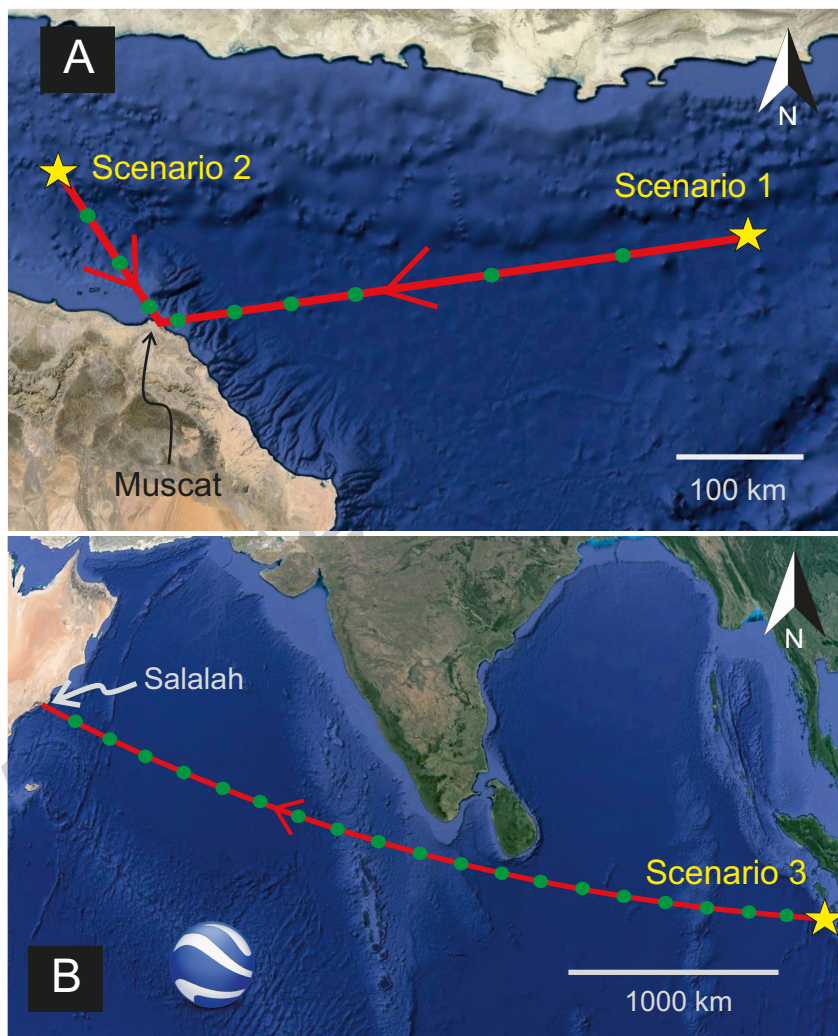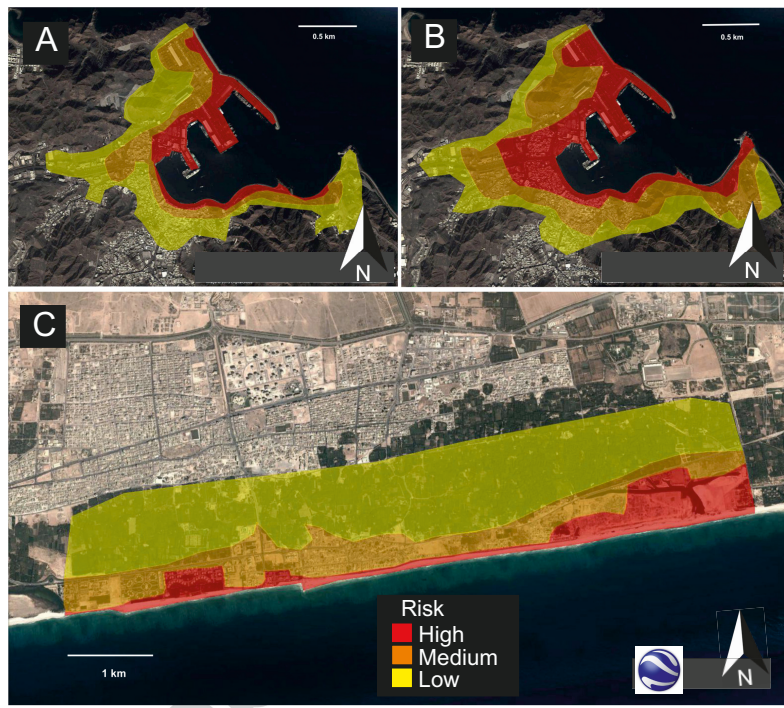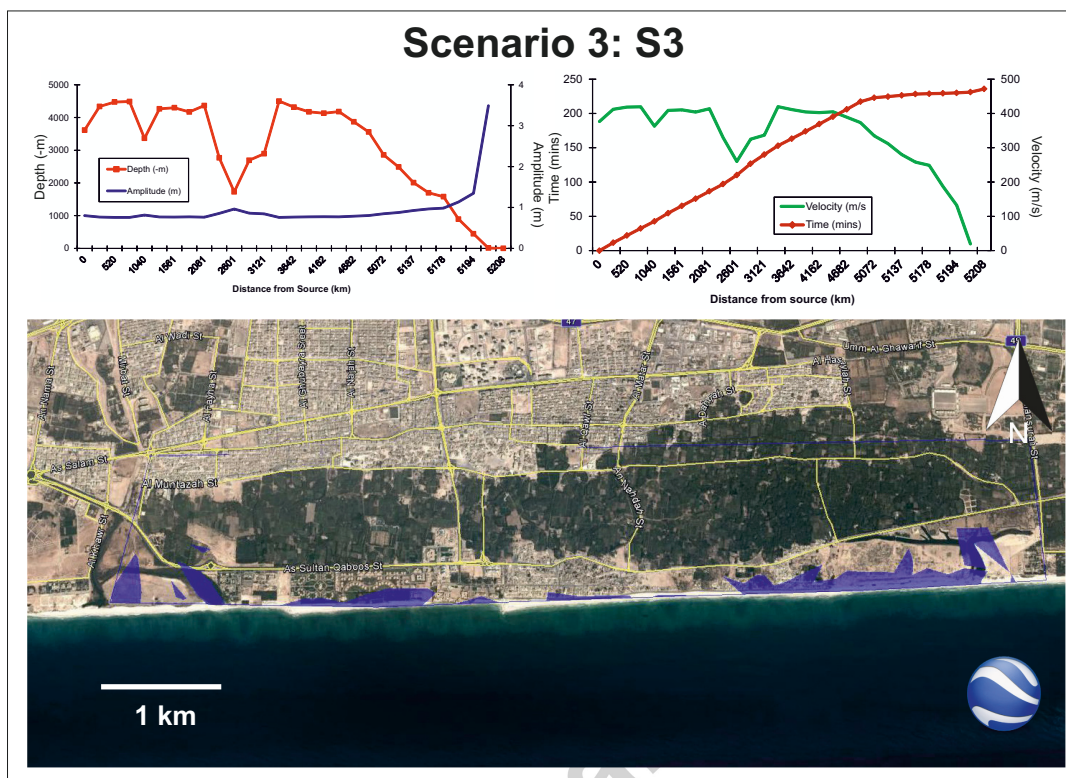
Scenario 3: S3

Scenario 2: S2

Scenario 1: S1